Journal of ELECTRONIC MATERIALS, Vol. 45, No. 11, 2016
DOI: 10.1007/s11664-016-4819-4

Photodiode Based on CdO Thin Films as Electron Transport Layer

M. SOYLU[1,2] and H.S. KADER[1]

1.—Department of Physics, Faculty of Sciences and Arts, Bingol University, Bingol, Turkey.
2.—e-mail: soylum74@yahoo.com

Cadmium oxide (CdO) thin films were synthesized by the sol–gel method. The films were analyzed by means of XRD, AFM, and UV/Vis spectrophotometry. X-ray diffraction patterns confirm that the films are formed from CdO with cubic crystal structure and consist of nano-particles. The energy gap of the prepared film was found to be 2.29 eV. The current–voltage (I–V) characteristics of the CdO/p-Si heterojunction were examined in the dark and under different illumination intensities. The heterojunction showed high rectifying behavior and a strong photoresponse. Main electrical parameters of the photodiode such as series and shunt resistances (R_s and R_{sh}), saturation current $I_{0,}$ and photocurrent I_{ph}, were extracted considering a single diode equivalent circuit of a photovoltaic cell. Results indicate that the application of CdO thin films as an electron transport layer on p-Si acts as a photodetector in the field of the UV/Visible.

Key words: CdO, illumination effect, electrical parameters

INTRODUCTION

Transparent conducting metal oxides (TCOs) are highly transparent in the visible region as well as a unique electrical property. Especially, cadmium oxide (CdO),[1,2] indium tin oxide (ITO) and [3] zinc oxide (ZnO)[4–6] have important places in the thin film technology. CdO thin films have a high transparency in the visible region. They have fundamental indirect gaps and direct allowed optical onset. The intrinsic direct band gap is due to the preparation method and the Burstein–Moss shift. The oxygen vacancies or Cd^+ ions generate donor states. This renders them n-type as semiconductors. Burbano et al.[7] reported that p-type CdO was not achievable, despite all growth conditions. Shallow donors in the CdO thin films will become responsible for V_o energy level, while in Ga_2O_3,[8] SnO_2,[9] In_2O_3,[10] and ZnO,[11] deep donors are found to be dominate for V_o.

CdO thin films were synthesized by various methods such as magnetron sputtering,[12] DC-activated reactive evaporation,[13] chemical bath deposition,[14] pulsed laser deposition,[15] spray pyrolysis,[16–21] and sol–gel.[22] Because CdO is synthesized to be a thin film, it can be used as the electron transport and blocking layer. Kim and Kwon[23] demonstrated that an energy barrier to keep injected electrons was formed via a CdO thin film in dye-sensitized solar cells (DSSCs). CdO has a high electrical conductivity and mobility value. It is an interesting material for optoelectronic applications because of its electron concentration higher than 10^{19} cm^{-3}. Combination by other semiconductor materials of nanostructured CdO thin films enhances the photocatalytic performance.[24] The electrical and optical properties of CdO thin films can be modified by doping of various metallic ions. Dakhel[25] investigated the electrical properties of Ge-doped CdO (CdO:Ge) films deposited on p-Si. Ge-doped CdO/p-Si heterojunctions exhibited a weak rectifying behavior. Khan et al.[26] reported that the CdO thin film exhibited a metallic property in a lower temperature region. A semiconducting behavior was observed for the whole measured temperature range with doping of Al. The carrier concentration of CdO thin film is of the order of 10^{21} cm^{-3}. n-type CdO thin film acts as carrier transport layer in combination with Si.

(Received April 8, 2016; accepted July 19, 2016; published online August 2, 2016)

In this study, nanostructured CdO thin films were prepared by the sol–gel method. Some special features of CdO films have been investigated using various techniques such as atomic force microscopy (AFM), x-ray diffraction (XRD) pattern and ultraviolet visible (UV–Vis) spectroscopy. The film was used as a photoanode-electron transport layer on the silicon. *p*–*n* junction-like structure was characterized by the light-dependent electrical measurements.

EXPERIMENTAL PROCEDURES

High purity (99.99%) cadmium acetate dihydrate was purchased commercially (Sigma Aldrich company). A sol–gel of CdO was prepared at the molar rate of 0.5. Soda-lime glass (SLG) substrate was cleaned to remove the contaminants, and, thus, to obtain high quality films. SLG substrate was boiled in H_2O, NH_3, and H_2O_2 (5:1:1) for 20 min at 85°C and then in H_2O, H_2O_2, and HCl (5:1:1) for 20 min at 80°C. A CdO thin film was deposited on glass substrate by the sol–gel spin coating method. The sample was then heated at 150°C for 5 min to remove the solvent and organic residuals. Finally, the sample was annealed at 400°C for 60 min in a furnace and then cooled to room temperature. The cleaning procedure was also repeated for *p*-type silicon wafer. To obtain the ohmic contact, aluminum (Al) was deposited on silicon substrate by means of thermal evaporation and exposed to a thermal treatment at 550°C for 5 min in N_2 atmosphere. The CdO film was deposited onto a *p*-Si wafer. After coating of CdO film, Al contacts were formed through a molybdenum mask with diameters of 1 mm. The crystal structure of the CdO thin film was characterized by XRD (Rigaku) using CuKα radiation. Surface morphology of the CdO thin film was evaluated using a PARK system XE 100E AFM (PSIA Corp., Korea). Optical data was obtained by UV–Vis spectroscopy (Shimadzu UV-VISNIR 3600 spectrophotometer). A LCRmeter (2400 Keithley) was used to obtain the electrical characteristics. The photoresponse characteristics were measured using a solar simulator (ABET class A, US patent 8116017).

RESULTS AND DISCUSSION

Structure, Surface and Optic Properties

The structural characterization of the CdO thin film is estimated by the XRD technique. Figure 1 shows the x-ray diffraction pattern of pure CdO thin film. Peaks define a cubic structure with the card number of JCPDS: 05-0640. Peak intensity at (111) is higher when compared with others. The lattice constant (a) is related to the crystal structure and calculated using the following relation:

$$\frac{1}{d_{hkl}^2} = \frac{4}{3}\left(\frac{h^2+k^2+hk}{a^2}\right) + \frac{l^2}{c^2}, \quad (1)$$

where d_{hkl} is interplanar spacing for planes and (hkl) is the Miller indices. The lattice constant of

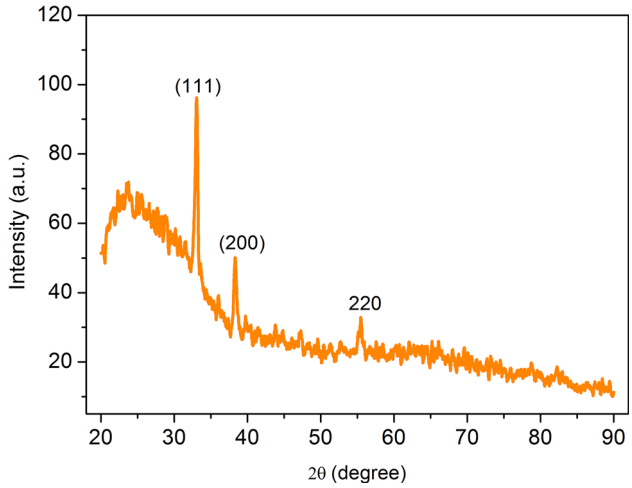

Fig. 1. XRD spectra of CdO thin film growth on glass substrate.

4.69 angstroms for the dominant peak of the CdO thin film is given in Table I, indicating a good agreement with the reported values.[27,28] Texture coefficients, ($TC_{(hkl)}$), which are defined as the preferential orientation of crystallographic planes, are expressed by equation[29]:

$$TC_{(hkl)} = \frac{I_{(hkl)}/I_{0(hkl)}}{N^{-1}\sum_N I_{(hkl)}/I_{0(hkl)}}, \quad (2)$$

where $I_{(hkl)}$ is the relative intensity of the plane (hkl), $I_{o(hkl)}$ the standard intensity, and N the number of reflections. The values of the texture coefficient of CdO thin films for the diffraction peak (111) and (200) are listed in Table I. It is seen that the value of $TC_{(111)}$ is greater than that of $TC_{(200)}$. The higher value of $TC_{(111)}$ implies a low-energy crystallographic plane. The particle size (D) can be calculated by the following equation[30,31]:

$$D = \frac{0.94\lambda}{B\cos\theta}, \quad (3)$$

where B is the full width at half maximum (FWHM) value, λ is the wavelength, and θ is the Bragg angle. The value of the average crystallite size (D) was found to be 35.02 nm, exhibiting a good crystallinity (Table I). Figure 2 shows AFM images of a CdO thin film. It consists of nano-sized particles. It is seen that the surface is homogeneously covered. Surface roughness (R_q) is a parameter of surface texture. The roughness parameter was calculated to be 116.32 nm, indicating the raw profile data. Smooth surfaces are an indicator of the device performance.

Optical features such as transmittance, absorbance, and reflectance are evaluated with an UV/Vis spectrophotometer. Figure 3a–c shows the optical measurements. The CdO thin film is transparent 80% above in the visible region. Reflectance spectra changes with wavelength and shows a wide peak after ~500 nm. Low reflectance becomes a crucial point for the performance of the photovoltaic

Table I. Some structural and optic parameters of CdO thin film

Molarity	2θ	FWHM	Texture coefficient (111)	Texture coefficient (200)	Average crystallite size (*D*) (nm)	Lattice constant (*a*) (Å)	E_g (eV) (PL)	R_q (nm)
0.5	33.02	0.272	2.560	1.701	35.02	4.6949	2.23	116.32

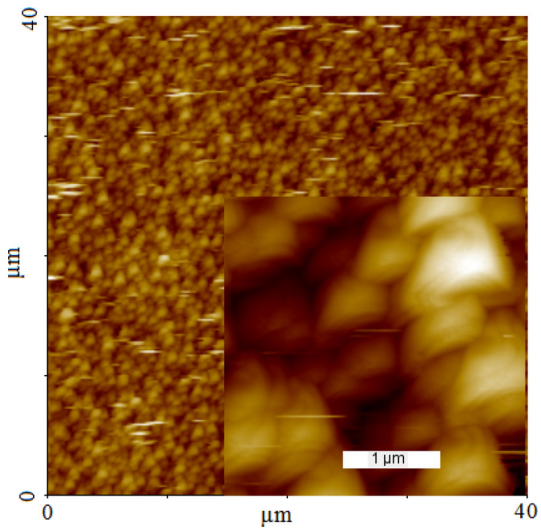

Fig. 2. AFM microphotograph in 40 × 40 μm^2 area of CdO thin film (inset shows the image of 5 × 5 μm^2 area).

application. The absorption edge is characterized by a blue shift. The optical band gap (E_g) is determined using the equation[32]:

$$\alpha h\nu = C(h\nu - E_g)^n, \quad (4)$$

where C is a constant coefficient, E_g is the optical band gap, and $h\nu$ the photon energy. Figure 4 shows the plot of $(\alpha h\nu)^2$ versus $h\nu$ for the CdO film. The optical band gap can be determined by extrapolating the linear portion of the plot of $(\alpha h\nu)^2$ versus $h\nu$. The value of E_g was found to be 2.29 eV. Photoluminescence spectroscopy is one of the ways of determining the semiconductor band gap.[33] Figure 5 shows the photoluminescence (PL) intensity versus wavelength for pure CdO thin film. The excitation wavelength is 325 nm. The approximated band gap of 2.23 eV is low when compared to that obtained from the optical absorption spectra (Table I).

Electrical Characteristics of CdO/*p*-Si Heterojunction

Energy band diagram of the heterojunction between CdO and Si semiconductor materials can be formed using the Anderson model.[34] Figure 6 shows the energy band diagram of the CdO/*p*-Si heterojunction. In this diagram, E_g(Si) = 1.12 eV, E_g(CdO) = 2.29 eV, χ(Si) = 4.05 eV, and χ(CdO) = 4.51 eV.[35] χ is the electron affinity. As it is seen in Fig. 6, the conduction-band offset is the difference between the electron affinities of semiconductors ($\Delta E_C = \chi(\text{CdO}) - \chi(\text{Si}) = 0.46$ eV) and the valance-band offset, ΔE_V, is 1.63 eV ($E_g(\text{CdO}) - E_g(\text{Si}) + \Delta E_C$). ΔE_V is higher than ΔE_C. The hole injection from *p*-Si to CdO is lower compared to the injection of electrons from CdO to *p*-Si. In this case, electrons are faced with a smaller potential barrier. The work function for the Al metal is 4.08 eV. This means that the work function of the Al metal is close to the electron affinity of the Si. A metal–semiconductor junction results in an ohmic contact if the barrier height is zero. Lee et al.[36] fabricated a transparent conducting inorganic (*n*-ZnO)/organic (*p*-type PEDOT:PSS) vertical heterojunction diode (Au/PEDOT:PSS/ZnO/In). They reported that the *I–V* characteristics showed the ohmic behavior between the Au/PEDOT and In/ZnO contact. The rectifying characteristics were attributed to the junction between *p*- and *n*-semiconductor layers.

Contacts with Al metal at the top and bottom exhibit ohmic *I–V* behavior, indicating that electrons can pass through the CdO thin film. The current–voltage (*I–V*) plots of the CdO/*p*-Si heterostructure under dark and various illumination intensities are shown in Fig. 7. The *I–V* characteristics for the heterojunction containing nanoparticles exhibit rectifying behavior and a significantly high rectification ratio (RR) of 8.4×10^5 at 2 V in dark conditions. The calculations (I_{fwd}/I_{rev}) based on *I–V* measurements also rationalize the voltage dependence of transport for the rectifying structure, since the forward bias (V_{fwd}) obtained is greater as compared to the reverse bias (V_{rev}). RR in different light intensities is presented in Table II. The turn-on voltage and the reverse leakage current were determined to be 0.62 V and 3.91×10^{-10} A, respectively. A device with a lower turn-on voltage deviates from the ideal *I–V* behavior. The turn-on voltages extracted by the dark and illumination intensity-dependent forward *I–V* curves do not remain constant.

The current (I) through a rectifying barrier is evaluated according to thermionic emission (TE) theory[37]:

$$I = I_o \exp\left(\frac{q(V - IR_s)}{nkT}\right), \quad (5)$$

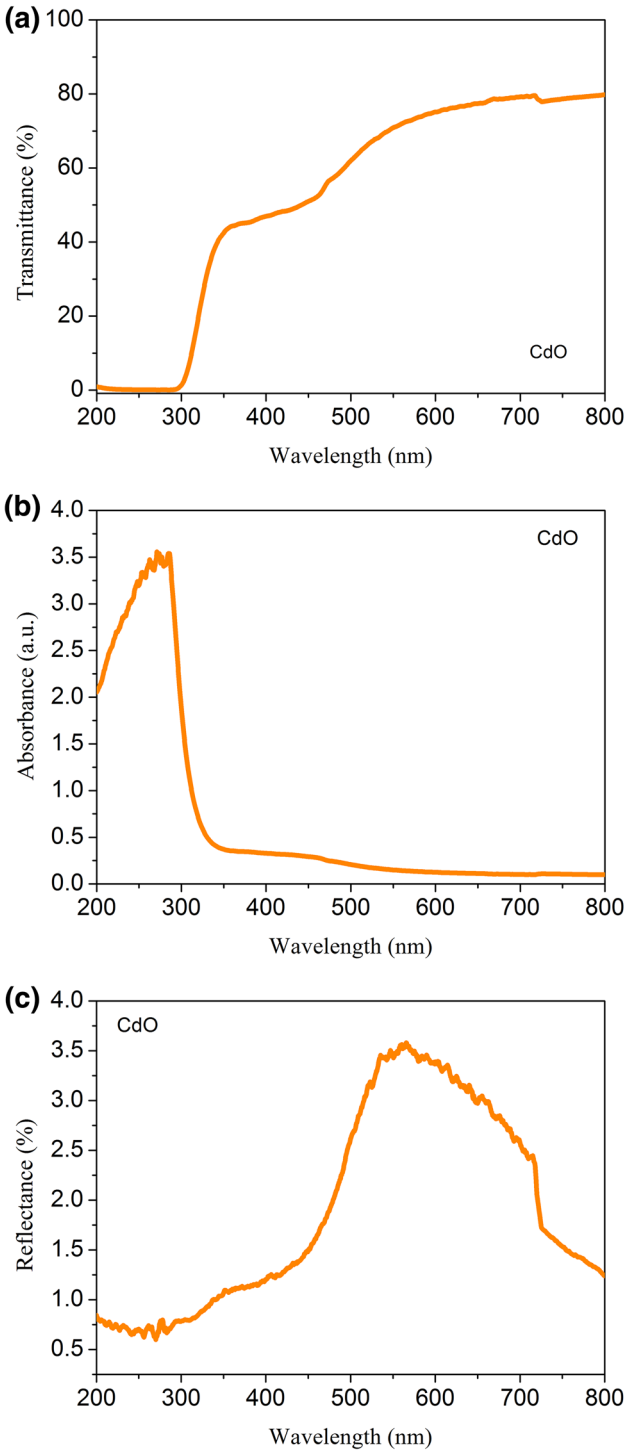

Fig. 3. (a) Transmittance, (b) absorbance and (c) reflectance spectra of CdO thin film.

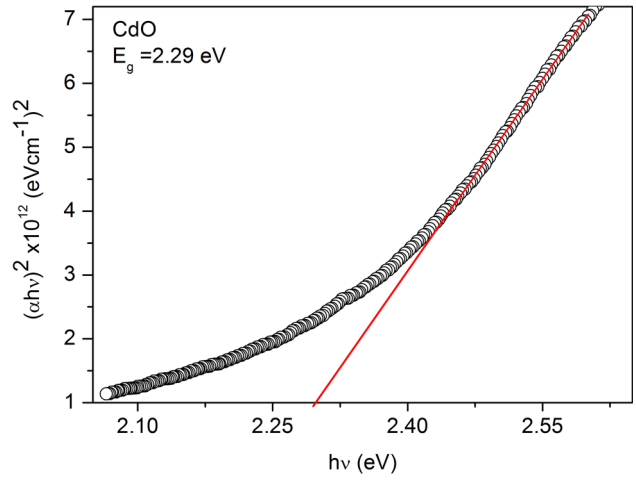

Fig. 4. Plot of $(\alpha h\nu)^2$ versus $h\nu$ for CdO thin film.

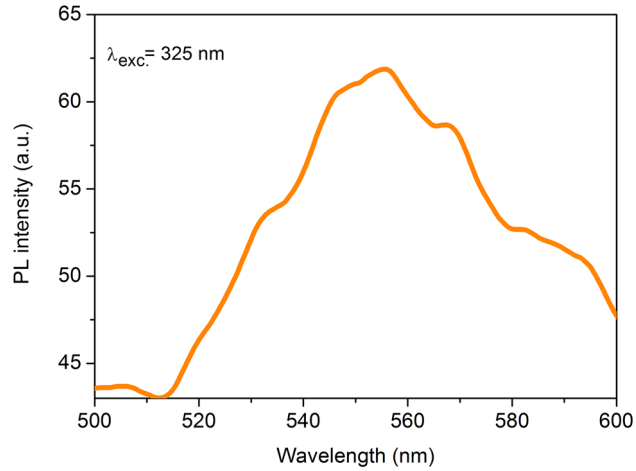

Fig. 5. PL spectra for CdO thin film.

where I_0 is the reverse saturation current given by:

$$I_0 = AA^*T^2 \exp\left(-\frac{q\Phi_b}{kT}\right), \quad (6)$$

where A is the effective area, q is the electronic charge, V is the forward-bias voltage, A^* is the Richardson constant, T is the absolute temperature, k is the Boltzmann constant, Φ_b is the barrier height, and n is the ideality factor. The values of n and Φ_b were determined from the slope and the intercept of the forward bias In(I) versus voltage (V) plot and found to be 1.43 and 1.03 eV, respectively, in dark conditions. A high barrier height was obtained at room temperature, confirming the barrier between semiconductor materials. Barrier heights and ideality factors are listed as a function of light intensity in Table II. The resulting measurements show a strong photoresponse. The reverse bias current increases with increasing illumination intensity (compared to dark conditions). The device exhibits the single-junction photovoltaic cell behavior. With the incident light, electrons are excited above the band gap and free electron–hole pairs occur. Even if the energy amount that penetrates to the junction is less than the band gap, a bound electron–hole pair is created, resulting in

an increase in the current. The barrier height decreases partly linearly with increasing light intensity (Fig. 8). $\Phi_{b0}(P) = \Phi_{b0} - \alpha P$, P is the intensity of illumination and α is the illumination coefficient. Here, $\alpha = -6.14 \times 10^{-4}$ eV/W. This value has the same order of magnitude of the temperature coefficient for the Si band gap (-4.73×10^{-4} eV/K).[38]

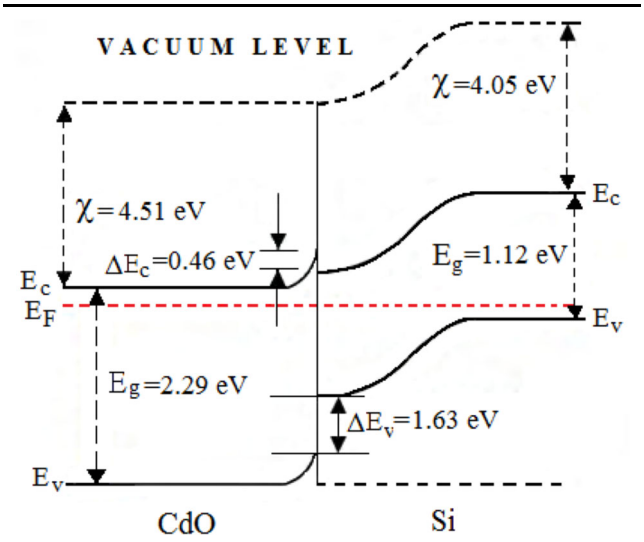

Fig. 6. Energy band diagram of heterojunction.

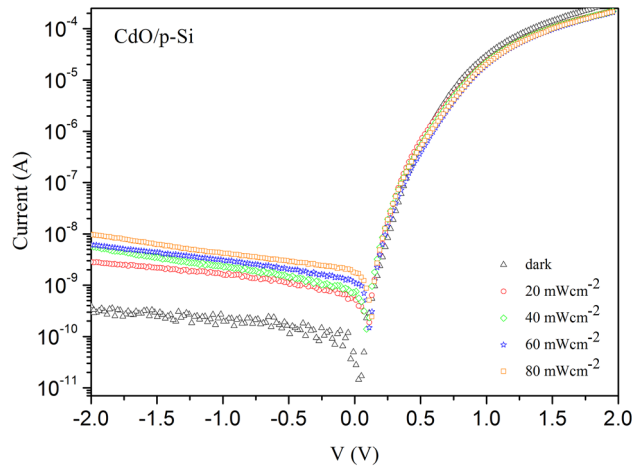

Fig. 7. The forward and reverse bias semi-logarithmic *I–V* characteristics of the Al/CdO/*p*-Si heterojunction diode in the dark and under various illumination intensities.

The variation in illumination intensity dependent photocurrent (I_{ph}) versus barrier height shows a nonlinearity. This effect can be described with the load resistance, the interface states, and the series resistance as well as others (i.e., biasing voltage, illumination conditions, the current-limiting barrier, thermal conditions, and the physical dimension of the device).

It is seen in Fig. 7 that the photocurrent, $I_{ph} = (I_{light} - I_{dark})$, where I_{light} is the current in the presence of light, while I_{dark} is the current in the absence of light, increases step by step with increasing illumination intensity. The photocurrent depends on the increasing illumination intensity. $I_{ph} = \kappa P^{\gamma}$, I_{ph} is the photocurrent, κ is a constant and γ is an exponent.[39] Figure 9 shows the variation of I_{ph} versus P. The value of γ was found to be $0.5 < \gamma < 1.0$. The localised states are assumed to arise from trap levels, indicating defects and impurities in the mobility gap.[40] Photons absorbed to generate photoelectrons and electrons collected in the dark display the current gain (g) from a fully linear dependence on illumination power.[41] The current gain is determined from the *I–V* characteristics using the equation:

$$\text{Gain} = \frac{I_{ph}}{I_{dark}}. \quad (7)$$

The g value was obtained to be 30.94 at a light intensity of 80 mW/cm^2, applying a bias voltage of 2 V. The saturation of the trap states leads to an increased gain at higher illumination power.[42] The performance of a photodiode depends on basically the photo-induced generation and transport of carriers. Higher dark current and photocurrent can be provided with better transport properties of the contact elements.

To examine the photovoltaic performance of the CdO/*p*-Si structure, the *J–V* measurements were performed using a power supply (voltage source). Figure 10 shows the photocurrent density–voltage characteristics (*J–V*) at irradiances of 20 mW/cm^2, 40 mW/cm^2, 60 mW/cm^2, and 80 mW/cm^2. We calculate the open-circuit voltage (V_{oc}) value of the *n*-/*p*-type photovoltaic cell using the equation:

$$V_{oc} = V_T \ln\left(\frac{J_{sc}}{J_0} + 1\right), \quad (8)$$

Table II. Illumination dependent values of various parameters determined from the *I–V* characteristics of a CdO/*p*-Si heterojunction

Power (mW/cm^2)	Φ_b (eV)	n	RR	R_s (Ω)	J_0 (mA/cm^2)	V_{oc} (mV)	FF (%)
0	1.03	1.43	8.40×10^5	1.24×10^5	1.24×10^{-8}	–	–
20	1.01	1.47	7.78×10^4	3.64×10^5	2.22×10^{-8}	28	20
40	0.99	1.60	3.81×10^4	7.94×10^5	5.73×10^{-8}	57	26
60	0.99	1.75	3.39×10^4	6.77×10^5	6.01×10^{-8}	96	34
80	0.97	1.86	2.25×10^4	1.91×10^5	1.06×10^{-7}	128	37

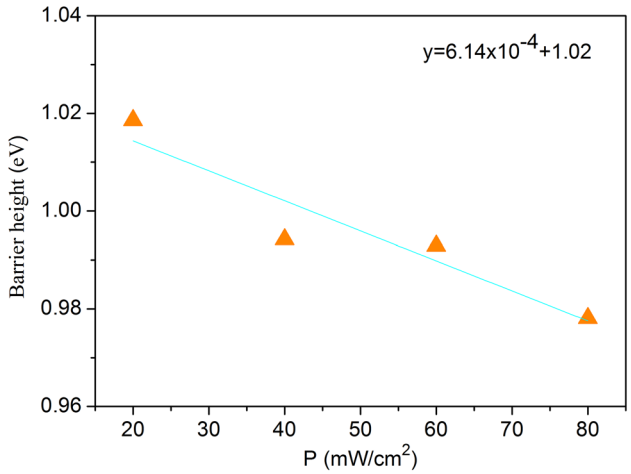

Fig. 8. Variation of barrier height versus P for an Al/CdO/p-Si heterojunction diode.

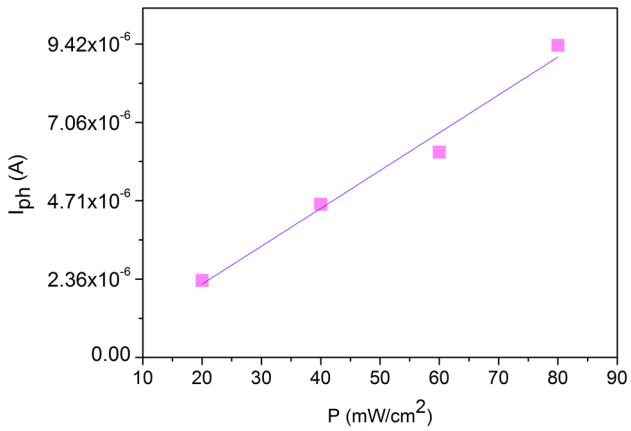

Fig. 9. Variation of I_{ph} versus P for an Al/CdO/p-Si heterojunction diode.

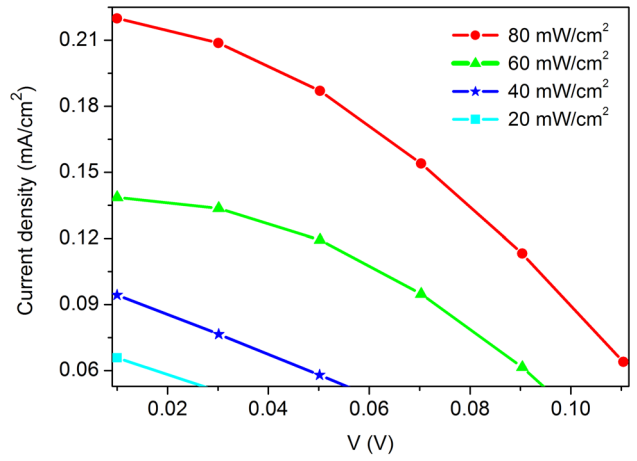

Fig. 10. Current density–voltage characteristics at irradiances of 20 mW/cm^2, 40 mW/cm^2, 60 mW/cm^2, and 80 mW/cm^2.

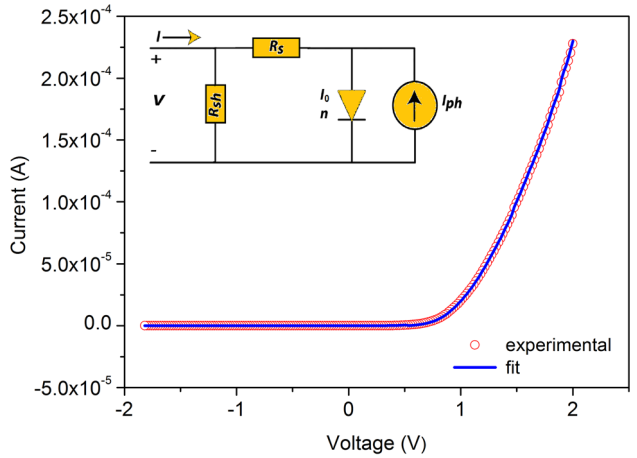

Fig. 11. I–V characteristics (open circle) with fitting curve (blue line) at an irradiance of 80 mW/cm^2. (Inset shows a diode equivalent circuit of the device including diode and parasitic resistances.).

where $V_T = 25.7$ mV is the thermal voltage at a temperature of 25°C. Some photovoltaic parameters are summarized in Table II. It is seen that the V_{oc} increases with increasing illumination intensity. The value V_{oc} of 128 mV can be judged to be inadequate for solar cell applications. However, the investigated diode can be used for developing a device that integrates optical sensing elements. A new method has been suggested to extract the photovoltaic parameters.[43–46] The current–voltage characteristics of an ideal photovoltaic cell are described by the well-known Shockley equation:

$$I_0 = \left(I_{sc} + \frac{R_s I_{sc} - V_{oc}}{R_{sh}}\right) \exp\left(-\frac{qV_{oc}}{nkT}\right) \quad (9)$$

$$I_{ph} = I_{sc} + \frac{R_s I_{sc}}{R_{sh}} - I_0, \quad (10)$$

where I_0, I_{ph}, R_s, and R_{sh} are the saturation current, photo current, series and shunt resistances, respectively. Figure 11 shows the I–V characteristics of a photovoltaic device with fitting curve (open circles and blue line indicate the experimental and fitted plots, respectively). Inset shows a diode equivalent circuit of the device containing parasitic and diode resistances. The resulting parameters for the photovoltaic cell were obtained from the fitting curve. In the light (intensity of 80 mW/cm^2), series and shunt resistances (R_s, R_{sh}) were found to be 2.1×10^5 Ω and 1.8×10^4 Ω, respectively. Also, to determine the series resistance, Norde[47] suggested an alternate way and defined the equation:

$$F(V) = \frac{V_0}{\xi} - \frac{kT}{q}\left(\frac{I(V)}{A^* A T^2}\right), \quad (11)$$

where ξ is the integer greater than n and dimensionless. Figure 12 shows the plots of $F(V)$ versus voltage. The barrier height (Φ_b) and the series resistance (R_s) can be found by the equation:

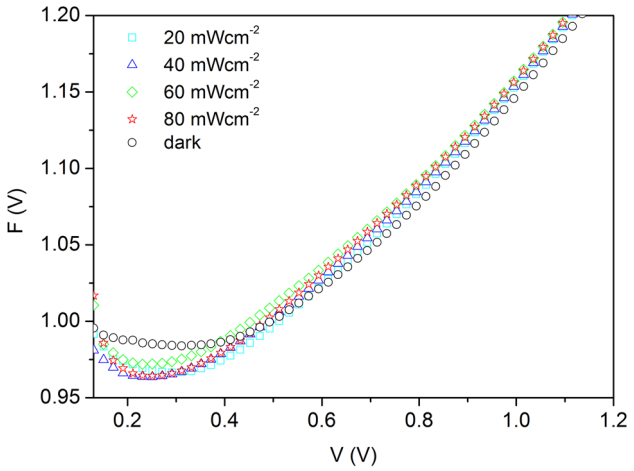

Fig. 12. Plots of $F(V)$ versus V.

$$\Phi_b = F(V_0) + \frac{V_0}{\xi} - \frac{kT}{q} \tag{12}$$

$$R_s = \frac{kT(\xi - n)}{qI_o}, \tag{13}$$

where $F(V_o)$ is the minimum point of $F(V)$. The values of R_s are listed in Table II. The values of series resistance obtained from fitting and Norde plots are in close agreement with each other.

CONCLUSIONS

CdO thin films were synthesized by the sol–gel method. The films were analyzed by means of XRD, AFM, and UV/Vis spectrophotometry. Measurements revealed the polycrystalline nature of the highly transparent conducting CdO film. The n-CdO/p-Si heterojunction diode was fabricated, and its photovoltaic performance was investigated. The heterojunction diode showed a high rectifying ratio and a strong photoresponse. CdO thin films seem to have the potential to contribute as the electron transport layer for a Si-based photodiode. Despite the weak solar cell performance, the heterojunction diode demonstrates a photoconducting behavior. Thus, the n-CdO/p-Si heterojunction can be used as a photodetector in the UV/Visible, improving the device quality.

ACKNOWLEDGEMENTS

This work was financially supported by the Scientific Research Projects Commission of Bingol University under Project Number BAP-38-201-2014.

REFERENCES

1. R. Ferro and J.A. Rodriguez, *Sol. Energy Mater. Sol. Cells* 64, 363 (2000).
2. R. Rajammal, V. Anbarasu, E. Savarimuthu, and S. Arumugam, *J. Electron. Mater.* 43, 3514 (2014).
3. S.B. Sapkota, A. Spies, B. Zimmermann, I. Dürr, and U. Würfel, *Sol. Energy Mater. Sol. Cells* 130, 144 (2014).
4. M. Caglar, S. Ilican, Y. Caglar, and F. Yakuphanoglu, *J. Mater. Sci. Mater. Electron.* 19, 704 (2008).
5. J. Zhong, S. Muthukumar, G. Saraf, H. Chen, Y. Chen, and Y. Lu, *J. Electron. Mater.* 33, 654 (2004).
6. S. Sharma, A. Tran, O. Nalamasu, and P.S. Dutta, *J. Electron. Mater.* 35, 1237 (2006).
7. M. Burbano, D.O. Scanlon, and Graeme W. Watson, *Am. Chem. Soc.* 133, 15065 (2011).
8. J.B. Varley, J.R. Weber, A. Janotti, and C.G.V. de Walle, *Appl. Phys. Lett.* 97, 142106 (2010).
9. A.K. Singh, A. Janotti, M. Scheffler, and C.G. Van de Walle, *Phys. Rev. Lett.* 101, 055502 (2008).
10. S. Lany and A. Zunger, *Phys. Rev. Lett.* 106, 069601 (2011).
11. S.J. Clark, J. Robertson, S. Lany, and A. Zunger, *Phys. Rev. B* 81, 115311 (2010).
12. K. Gurumurugan, D. Mangalaraj, and S.K. Narayandas, *J. Electron. Mater.* 25, 765 (1996).
13. C. Sravani, K.T. Ramakrishna Reddy, and P.J. Reddy, *Semicond. Sci. Technol.* 6, 1036 (1991).
14. G. Phatak and R. Lal, *Thin Solid Films* 245, 17 (1994).
15. A.J. Varkey and A.F. Fort, *Thin Solid Films* 239, 211 (1994).
16. M. Yan, M. Lane, C.R. Kannewurf, and R.P.H. Chang, *Appl. Phys. Lett.* 78, 2342 (2001).
17. K. Gurumurugan, D. Mangalaraj, and S.K. Narayandass, *J. Cryst. Growth* 147, 355 (1995).
18. C. Saravani, K.T.R. Reddy, P.S. Reddy, and P.J. Reddy, *J. Mater. Sci. Lett.* 13, 1045 (1994).
19. L.C.S. Murthy and K.S.R.K. Rao, *Bull. Mater. Sci.* 22, 953 (1999).
20. H. Tabet-Derrazn, N. Benramdane, D. Nacer, A. Bouzidi, and M. Medles, *Sol. Energy Mater. Sol. Cells* 73, 249 (2002).
21. K. Sankarasubramanian, P. Soundarrajan, K. Sethuraman, R.R. Babu, and K. Ramamurthi, *Superlattices Microstruct.* 69, 29 (2014).
22. R.S. Mane, H.M. Pathan, C.D. Lokhande, and S.H. Han, *Sol. Energy* 80, 185 (2006).
23. M.-H. Kim and Y.-U. Kwo, *J. Phys. Chem. C* 113, 17176 (2009).
24. R. Suarez-Parra, I. Hernandez-Perez, M.E. Rincon, S. Lopez Ayala, and M.C. Roldan-Ahumada, *Sol. Energy Mater. Sol. Cells* 76, 189 (2003).
25. A.A. Dakhel, *Solid State Sci.* 25, 33 (2013).
26. M.K.R. Khan, M.A. Rahman, M. Shahjahan, M.M. Rahman, M.A. Hakim, D.K. Saha, and J.U. Khan, *Curr. Appl. Phys.* 10, 790 (2010).
27. R.W.J. Wyckoff, *Crystal Structure*, 2nd ed. (New York: Wiley, 1963).
28. W.J. Wang, X.J. Xie, J.Y. Liu, and K.H. Gao, *Solid State Commun.* 239, 1 (2016).
29. B. Benhaoua, A. Rahel, and S. Benramache, *Superlattices Microstruct.* 68, 38 (2014).
30. R. Ghosh, D. Basak, and S. Fujihara, *J. Appl. Phys.* 96, 2689 (2004).
31. K.R. Murali, A. Kalivanan, S. Perumal, and N.N. Pillali, *J. Alloys Compd.* 503, 350 (2010).
32. N.F. Mott and R.W. Gurney, *Electronic Processes in Ionic Crystals* (London: Oxford University Press, 1940).
33. P.G. Eliseev, M. Osinski, J. Lee, T. Sugahara, and S. Sakai, *J. Electron. Mater.* 29, 332 (2000).
34. G. Milnes and D.L. Feucht, *Heterojunctions and Metal–Semiconductor Junctions* (New York: Academic, 1972).
35. N.E. Makori, I.A. Amatalo, P.M. Karimi, and W.K. Njoroge, *Int. J. Optoelectron. Eng.* 4, 11 (2014).
36. D.-H. Lee, D.-H. Park, S. Kim, and S.Y. Lee, *Thin Solid Films* 519, 5658 (2011).
37. E.H. Rhoderick and R.H. Williams, *Metal–Semiconductor Contacts*, 2nd ed. (Oxford: Clarendon Press, 1988).
38. M. Soylu, A.A. Al-Ghamdi, and F. Yakuphanoglu, *Microelectron. Eng.* 99, 50 (2012).
39. S. Kazim, V. Ali, M. Zulfequar, M.M. Haq, and M. Husain, *Phys. B* 393, 310 (2007).
40. N. Camaioni, G. Casalbore-Miceli, G. Beggiato, M. Cristani, and C. Summonte, *Thin Solid Films* 366, 211 (2000).
41. N.K. Hassan, M.R. Hashim, and N.K. Allam, *Sens. Actuators A* 192, 124 (2013).

42. J.O. Island, S.I. Blanter, M. Buscema, H.S.J. van der Zant, and A. Castellanos-Gomez, *Nano Lett.* 15, 7853 (2015).
43. A. Ortiz-Conde, F.J.G. Sánchez, and J. Muci, *Sol. Energy Mater. Sol. Cells* 90, 352 (2006).
44. C. Zhang, J. Zhang, Y. Hao, Z. Lin, and C. Zhu, *J. Appl. Phys.* 110, 064504 (2011).
45. W. Jung and M. Guziewicz, *Mater. Sci. Eng. B* 165, 57 (2009).
46. W. Dawidowski, B. Sciana, I.Z. Lindert, M. Mikolášek, K. Bielaka, M. Badura, D. Pucicki, D. Radziewicz, J. Kovác, and M. Tłaczała, *Solid-State Electron.* 120, 13 (2016).
47. H. Norde, *J. Appl. Phys.* 50, 5052 (1979).